Colloid and Polymer Science (2024) 302:1081–1095
https://doi.org/10.1007/s00396-024-05249-8

RESEARCH

The relationship between chemical microstructure, crystallinity, mechanical properties, and CO_2/N_2 gases permselectivity of thermoplastic polyurethane membranes

Reza Abedi[1] · Behnaz Memar Maher[1] · Leila Amirkhani[1] · Mostafa Rezaei[2] · Sona Jamshidi[3]

Received: 13 January 2024 / Revised: 8 March 2024 / Accepted: 12 March 2024 / Published online: 8 April 2024

Abstract

This research investigated the synthesis of thermoplastic polyurethane (TPU) with a hard segment content (HSC) of 30% weight. The chain extender, the polyols, and the diisocyanate utilized 1,4-butanediol (BDO), and the polycaprolactone diol (PCL-diol) with molecular weights of 2000, 4000, and 10,000 and isophorone diisocyanate (IPDI), respectively. Differential scanning calorimetry (DSC), Fourier-transform infrared spectroscopy (FTIR), hydrogen nuclear magnetic resonance (^{1}H-NMR), and X-ray diffraction (XRD) were used to examine the chemical microstructure and physical properties of PCL diol and thermoplastic polyurethanes (TPUs). The molecular weight of the PCL diol as soft segments affected the crystallinity and glass transition temperature (T_g) of TPUs. An increase in PCL diol molecular weight resulted in a reduction in elongation at failure and an increase in ultimate tensile strength. This study was conducted to investigate the permeability and the permselectivity of CO_2 and N_2 gases over pressure ranges (3 to 9 atm). It was determined that the gas permeability of each sample increased in response to an increase in the pressure of the supplying gas. An elevation in the molecular weight of PCL-diols in TPU samples resulted in a reduction in selectivity and an increase in CO_2 and N_2 gas permeability. Although IPDI is a non-aromatic cyclic diisocyanate with a significant impact on thermoplastic polyurethane phase morphology, the goal of this paper is to create a change in the molecular weight of PCL-diol and investigate the effect of molecular weight on the resulting morphology as well.

Keywords Thermoplastic polyurethane (TPU) · Membrane · Permselectivity · Mechanical properties · Polycaprolactone · Crystallinity

Introduction

Membrane separation technology is a contemporary method of separation technology created in the past several decades. Air pollution has emerged as a substantial obstacle, causing detrimental effects on both human health and the environment. Various methodologies have been employed in research endeavors to eliminate noxious gases. One of the most prevalent methods for separating gases is the membrane. The efficacy of the membrane relies on its components and fabrication techniques. Most membranes utilized in industries are composed of polymers [1, 2]. Membrane technology is widely employed in several industrial applications, with gas separation being prominent. This technique dehumidifies air and removes organic gases from air streams, particularly in air and natural gas treatment. Different kinds of dense and porous membranes can be considered as gas separators [3, 4]. Gas separation membranes work differently depending on the type of material they are made of (polymeric or non-polymeric) [5–9], their structure [9–14], and shape [15–17]. Most polymers exhibit deficiencies in characteristics such as low-temperature flexibility, air permeability, and fatigue resistance, which impair their performance under varying temperature settings. Thermoplastic polyurethane (TPU) exhibits favorable characteristics in this domain, such as adequate temperature resistance, excellent

✉ Behnaz Memar Maher
be.maher@iau.ac.ir

[1] Department of Chemical Engineering, Ahar Branch, Islamic Azad University, Ahar, Iran

[2] Faculty of Polymer Engineering, Sahand University of Technology, Tabriz, Iran

[3] Department of Chemical Engineering, Tabriz Branch, Islamic Azad University, Tabriz, Iran

erosion resistance, strong mechanical resilience, and, in certain instances, appropriate biodegradability [18–21].

Thermoplastic polyurethanes (TPU) is a polymer used in membrane applications [22–24]. Polyurethanes have a microphase-separated structure, which affects the penetration of gases, and different gases can be dispersed across the phases. One of the key justifications for utilizing TPU in membrane applications is due to these stages [25–27]. TPUs, or thermoplastic polyurethanes, are a type of thermoplastic elastomer commonly made using traditional methods. They are utilized to produce thermoplastic polymers [6, 7, 17]. TPUs exhibit a rubber-like characteristic that has been treated like thermoplastic materials [17, 27, 28]. TPU typically consists of a segmented polymer structure, with hard and soft domains arranged alternately along the polymer chain. The polyol part of the soft segment gives the polymer its elasticity and flexibility. On the other hand, the hard segment, which comprises the urethane link between diisocyanate and diamine, or diol, makes the polymer stronger [10, 11, 23, 26]. The effectiveness of the TPU membrane relies on various factors, including the hydrogen bonding index (HBI), molecular weight, molar ratio of isocyanate and polyol, hard segment content (HSC), degree of crystallinity, polymer chain orientation, glass transition temperature, and degree of cross-linking. Literature reviews state that there is a relationship between the increase in the gas permeability and the kind of polyol and the strength of hydrogen bond as well [8, 15, 25, 26].

The stoichiometric ratio and the NCO/OH ratio play a crucial role in synthesizing thermoplastic polyurethane. These ratios are essential for regulating the synthesis conditions and determining the mechanical properties of the end products. The final polymer structure can be achieved by the specific molar ratio of –NCO and –OH, as the involved components react with each other in a stoichiometric manner with high efficiency [6, 7, 17]. TPU can be synthesized using two methods: pre-polymerization and one-step techniques. The pre-polymerization process involves the synthesis of a prepolymer through the reaction between a polyol and an isocyanate [7, 17, 29].

Consequently, the prepolymer terminates with –NCO at the end of its chain. Subsequently, the prepolymer reacts with a chain extender to achieve the final polymer. This kind of polymer can be produced through melting polymerization or using a suitable solvent [7, 17, 29].

TPU is applicable in the fabrication of membranes for gas separation. The penetration of gas into dense membranes occurs in three stages: the adsorption of gas molecules on the membrane surface, the diffusion of gas molecules through the membrane, and the desorption of gas molecules via the outer surface of the membrane [7, 10, 13]. Various factors influence permeability, with gas pressure being one of them. As mentioned earlier, the permeability of nitrogen remains constant as pressure increases. Conversely, the permeability of methane decreases as pressure increases, while an increase in pressure results in an increase in carbon dioxide permeability. The carbon dioxide permeability in polyurethane is increased due to the breakdown of this gas within the polymer [13–16].

The synthesis of TPU was conducted using the pre-polymerization approach, and its membranes were made by the solution casting route. It distinguishes itself from other research by modifying the duration of the reaction and the process of incorporating materials. X-Ray diffraction (XRD) patterns were utilized to assess the crystalline structure of thermoplastic polyurethane (TPU). The thermal properties of the samples were analyzed using DSC analysis, while their chemical structure was studied using ^{1}H-NMR. The mechanical qualities were assessed using the tensile test, while CO_2 and N_2 permeation tests evaluated the gas permeability properties.

In previous studies, the potential of TPU for use in the preparation of membranes was investigated [17, 19]. Polyurethane/poly(vinyl alcohol) (PU/PVA) membrane was used for gas separation [17]. In another study, poly(urethane-urea) (PUU) membranes based on contributing hard segments in gas separation were prepared using two bulky chain extenders, polytetramethylene-glycol, isophorone, and hexamethylene-diisocyanate [19].

In this study, novel poly(urethane-urea) membranes containing polyol (polycaprolactone diol) as polyol with different molecular weights were developed as the aim of a structure–property relationship study to enhance gas permeation. This research attempts to find the best range of molecular weights by taking the relationship between different PCL-diol molecular weights and the TPU membrane's ability to let gases move through it into consideration. An attempt has also been made to establish the correlation between chemical and physical properties, such as the hydrogen bonding index (HBI), degree of crystallinity, glass transition temperature, stress–strain, and gas permeability of TPU membranes. This study has utilized underexplored raw materials and synthesized all PCL-diols to enhance precision. Although IPDI is a non-aromatic cyclic diisocyanate with a significant impact on thermoplastic polyurethane phase morphology, the goal of this paper is to change the molecular weight of PCL-diol and investigate the effect of molecular weight on the resulting morphology as well. This paper aimed to utilize various molecular weights of PCL-diol in the production of TPU while keeping the conditions the same. To achieve this, the molecular weight of PCL-diol had to be measured more accurately.

Experimental

Materials

Isophorone diisocyanate (IPDI, M_W: 222.3 g/mol), 1,4-butanediol (BDO, $C_4H_{10}O_2$, M_W: 90.122 g/mol),

Table 1 The number of precursors for PCL-diol synthesis

Molecular weight (g/mol)	Toluene (mL)	Stannous octoate (g)	BDO (g)	ε-Caprolactone (g)
2000	35	0.091	0.897	19.261
4000	35	0.047	0.449	19.261
10,000	35	0.0185	0.184	19.261

ε-caprolactone (CL, $C_6H_{10}O_2$, M_W: 114.14 g/mol), dibutyltin dilaurate (DBTDL, $C_{32}H_{64}O_4Sn$, M_W: 631.56 g/mol), Tin (II) 2-ethyl hexanoate or stannous octoate (Sn $(Oct)_2$, $C_{16}H_{30}O_4Sn$, M_W: 405.122 g/mol), dimethylformamide (DMF, M_W: 73.09 g/mol), and toluene (C_7H_8, M_W: 92.141 g/mol) were purchased from Merck Co., Germany. CO_2 and N_2 gas with a purity of 99.95 mol% were supplied by the Barfab Co., Iran.

PCL-diol synthesis

Polycaprolactone diol (PCL-diol) was synthesized by the ring-opening polymerization method [29–32]. As a representative, for the synthesis of 20 g PCL-diol (M_W: 2000 g/mol), toluene (35 mL) as solvent was mixed with stannous octoate as catalyst (0.225 mmol, 0.091 g) and BDO as the initiator (9.98 mmol, 0.88 mL), then poured in a three-neck flask at 90 °C and mixed for 30 min. After that, ε-caprolactone monomer (0.175 mol, 18.6 mL) was added and mixed at 110 °C for 24 h to complete the reaction. All processes were done under an N_2 atmosphere. To precipitate PCL-diol, methanol at a ratio of 10:1 (V/V) relative to the polymer solution was used and the product was dried at 50 °C in a vacuum oven for 24 h. ^{1}H-NMR analysis was used to determine its molecular weight. The following recipes (Table 1) were used to synthesize PCL-diol with various molecular weights [29].

TPU synthesis

To investigate the effects of the PCL-diol soft segment's molecular weight on TPU final properties, polyurethanes were synthesized with different molecular weights of PCL-diol. However, in all the synthesized samples, the NCO/OH ratio was kept at one by changing the molar ratio of raw materials. For the synthesis of TPU with 30wt.% hard segment content (HSC), three types of PCL-diols with molecular weights of 2000, 4000, and 10,000 g/mol were used as a polyol, IPDI as diisocyanate, BDO as chain extender, and DBTDL as the catalyst [14, 15, 21]. The prepolymerization method was used for TPU synthesis. In this method, the desired amount of PCL-diol and DBTDL was mixed with toluene as a solvent with a mass ratio of 1 to 2, and IPDI was added to the mixture in a three-neck flask immersed in an oil bath at a temperature range of 80 to 90 °C and stirring speed of 300 rpm for 24 h. Since IPDI has the lowest chemical reaction rate among other isocyanates, the synthesis of TPU based on IPDI takes longer. For this reason, more time must be considered for TPU synthesis [6, 7, 18]. The desired amount of BDO was added to the solution as a chain extender to complete the polymerization process. After 4 h, the resultant polymer was placed in a vacuum oven at 110 °C for 48 h. The molar ratio of the precursors is presented in Table 2. The reaction scheme to synthesize TPUs is demonstrated in Fig. 1.

The solution casting method for the preparation of TPU membranes

The solution casting approach was used to create the membrane. In this method, the polymer solution is poured into a mold, and a membrane is formed after the evaporation of the solvent. The utilization of a hot press for membrane preparation results in the formation of minute bubbles, uneven thickness, and the inability to achieve the necessary thickness [18–21].

Membranes were prepared with a thickness of 150 to 200 µm and a diameter of 8 cm. The membrane was prepared by dissolving 1 g of TPU in 10 mL of DMF at 80 to 90 °C for 24 h while churning at 300 rpm. After pouring the solution into a Teflon mold, it was left at room temperature to settle for 2 days to reach temperature stability, remove small bubbles caused by rapid evaporation of solvents, and achieve film uniformity [19, 20, 22]. Finally, the membrane was placed in the vacuum oven with a fan at 60 °C to evaporate the solvent for 24 h. Then, the membrane was removed

Table 2 The molar ratio of TPU precursors

Sample	IPDI		PCL diol		BDO		HSC (%)
	Molar ratio	Mass (g)	Molar ratio	Mass (g)	Molar ratio	Mass (g)	
TPU 2000	3.445	1.665	1	5	2.445	0.480	30
TPU 4000	6.485	1.602	1	5	5.485	0.549	30
TPU 10000	15.150	1.981	1	5	14.150	0.750	30
Catalyst: 2.3×10^{-7} mol/cm^3							

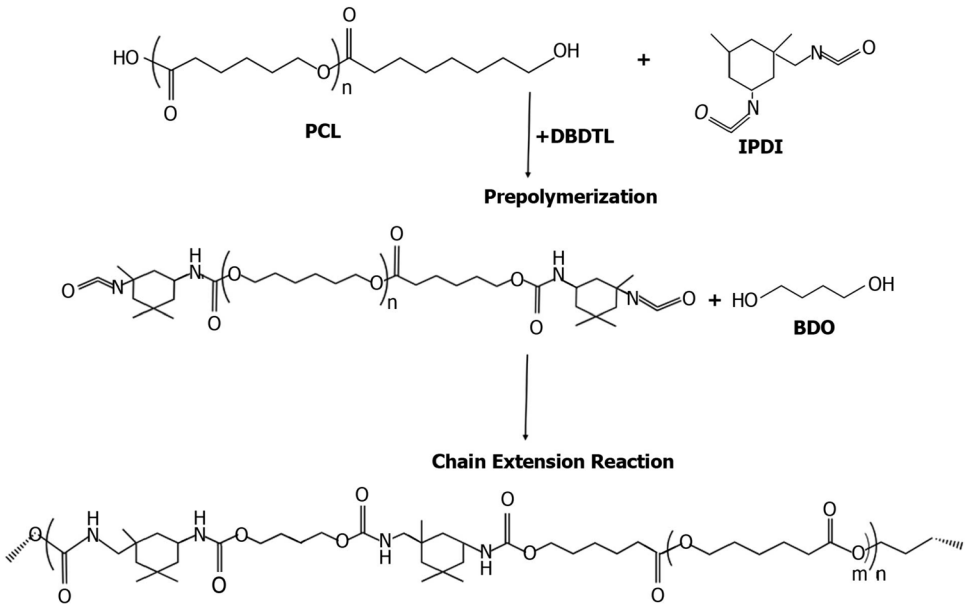

Fig. 1 Schematic synthesis route for the preparation of TPU

from the mold. To ensure the absence of solvent and stabilize the membrane, it was placed in a vacuum oven with a fan at a temperature of 60 °C for 24 h [19, 20, 22].

Characterization methods

The chemical structure of synthesized PCL-diols with various molecular weights and TPUs was characterized via ^{1}H-NMR spectroscopy. ^{1}H-NMR analyses were recorded at 25 °C with a Bruker 400 MHz spectrometer (Ultra Shield 400, Germany). As a solvent, deuterated chloroform ($CDCl_3$) was utilized, and chemical shifts were measured using tetramethyl silane (TMS) as the internal standard. The molecular weight of the produced PCL-diols was calculated using Eq. (1) [29, 33–35]:

$$X_{SS} = 2 \times \frac{A(\delta_D)}{A(\delta_E)}, M_n = \left(X_{SS} \times 114.14\right) + 262 \quad (1)$$

where X_{SS} is the ratio of the areas corresponding to the peaks at the resonances of δ_D and δ_E, and M_n is the number average molecular weight of PCL-diol.

Fourier-transform infrared spectroscopy (FTIR) spectra were recorded using a Bruker FTIR spectrometer (Tensor 27, Germany) measuring 600 to 4000 cm^{-1}. The pellets of PCL-diol samples were recorded in FTIR mode, and the film of TPU samples was recorded in ATR-FTIR mode. The hydrogen bonding index (HBI) was calculated using the ratio of the area under the peaks and Eq. (2) [29]:

$$HBI\ (\%) = \frac{A_{c=o\ bonded}}{A_{c=o\ bonded} + A_{c=o\ free}} \times 100 \quad (2)$$

where HBI (%) is the number of hydrogen-bonded carbonyl groups, $A_{C=O\ bonded}$ is the surface area under the peak corresponding to hydrogen-bonded carbonyl groups, and $A_{C=O\ free}$ is the surface area under the peak corresponding to free carbonyl groups.

DSC (Netzsch DSC-200 F3, Germany) thermal analysis was used to characterize and determine the transition temperatures of PCL-diols and TPUs. For this purpose, 5 mg of the synthesized materials was heated using a DSC device in the temperature range of − 100 to 250 °C with a heating rate of 10 °C/min. The samples' crystallinity (% X_c) was calculated using the heat of fusion of PCL-diol of 100% crystalline PCL-diol (136 J/g). Equations (3) and (4) are used to calculate the degree of crystallinity of PCL-diol and TPUs, respectively [32–35].

$$X_S(\%) = \frac{\Delta H_{SS}}{136} \times 100 \quad (3)$$

$$X_S(\%) = \frac{\Delta H_{SS}}{\Delta H_C \times (1 - HS)} \times 100 \quad (4)$$

Here, ΔH_{SS} is the soft segment's heat of fusion (J/g) and H_S is the normalized mass of the hard segments. ΔH_{SS} in Eq. (3) is the heat of fusion calculated by Fig. 2a. It is the surface area on the melting point peak of PCL-diol crystals calculated from the DSC diagram. ΔH_{SS} in Eq. (4) is the heat of fusion calculated by Fig. 2b. It is the surface area on the melting point peak of TPU crystals calculated from the DSC diagram, where ΔH_C is calculated by the DSC thermogram from the melting point peak of TPU crystals. That HS is the amount of the hard part, which is fixed at 30 wt.% for all TPUs. For TPU in Fig. 2b, any transition has not been

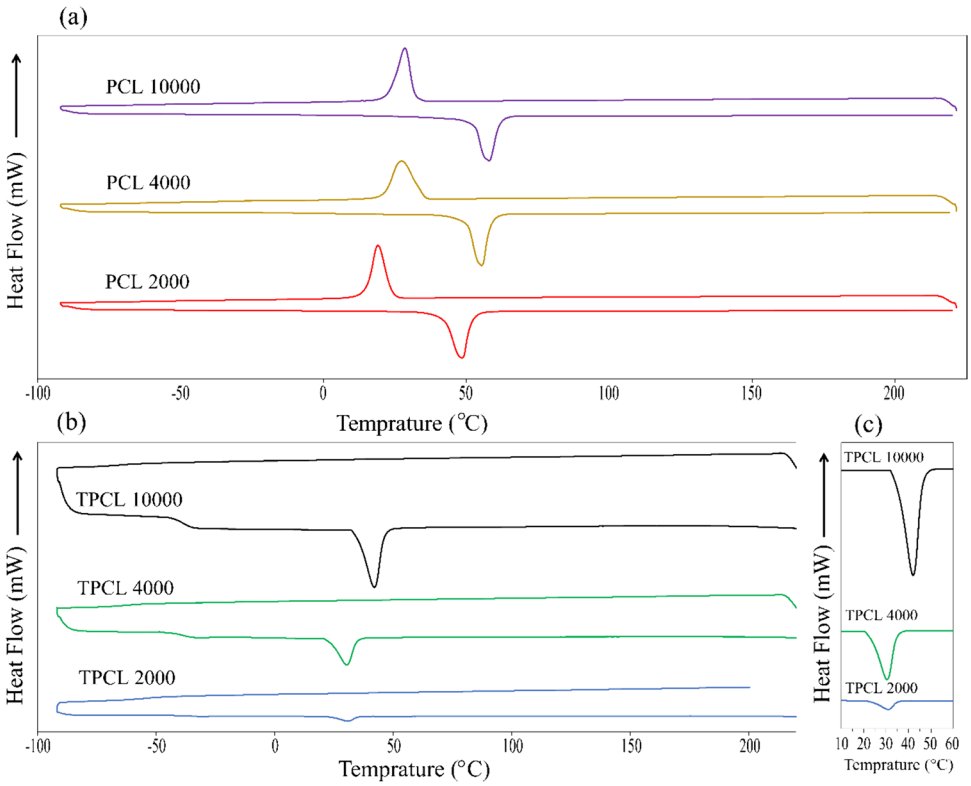

Fig. 2 The DSC thermograms of synthesized PCL-diols (**a**) and TPUs (**b**) and melting point (T_m) (**c**)

seen for the hard phase at a temperature until 200 °C. For this reason, Eqs. (3) and (4) focused more on the soft part [32–35].

X-Ray diffraction (XRD) patterns of samples were acquired by an X-ray diffractometer (Siemens D5000, Germany) using a copper anode with an accelerating voltage of 35 kV and a current of 20 mA. Samples were scanned in the range $2\theta = (10–50)°$ at ambient temperature and a rate of 0.01 s/step. Equation (5) was used to calculate the samples' crystallinity degree and the High Score Plus software was applied to analyze to XRD's peaks [33–35].

$$X_c(\%) = \frac{A_{110} + A_{111} + A_{200}}{A_{110} + A_{111} + A_{200} + A_{ah}} \times 100 \quad (5)$$

Here, A_{hkl} is the area of the crystal plates (hkl) in XRD patterns, and A_{ah} corresponds to the amorphous halo. Equation (6) is used to measure 110, 111, and 200 crystal plate sizes [33–35]. It should be noted that the area was measured under the XRD patterns diagram using PeakFit software.

$$L_{hkl} = \frac{K \times \lambda}{\beta_{hkl} \times cos\theta_{hkl}} \quad (6)$$

Here, L_{hkl} is the size of the crystal plate (hkl), K is the Scherer constant ($K = 0.9$), β is the full-width diffraction at half maximum (FWHM), and λ and θ is the X-ray wavelengths (equal to 0.01540 nm) and Bragg's angle, respectively [33–35].

The mechanical properties of TPU membranes were determined by the Zwick/Roell machine (Z010, Germany). In this analysis, the pre-load value was 0.5 N, and the tensile rate was 10 mm/min according to the ASTM D 882 standard. At least three specimens of each sample were tested.

The hard segment content of synthesized TPUs was calculated by Eq. (7). As written, in the structure of TPUs, PCL-diol is the soft segment, and the remaining parts of IPDI and BDO are known as the hard segment. As stated, the quantity of HSC in each sample is assumed to be 30% and remains constant; Eq. (7) is used accordingly. Indeed, it is presumed that the molar ratio of PCL-diol remains constant at one and that its mass is 5 g. The other substances' molar ratio and mass are estimated using molecular weight and the provided equation [29, 33–35].

$$HSC(\%) = \frac{(n_{IPDI} \times M_{IPDI}) + (n_{BDO} \times M_{BDO})}{(n_{IPDI} \times M_{IPDI}) + (n_{BDO} \times M_{BDO}) + (n_{PCL-DIOL} \times M_{PCL-DIOL})} \quad (7)$$

Here, M is the M_W of the precursors and n is the molar ratio of the precursors. Table 2 displays the molar ratio and the weight amount of the precursors. The molecular weight of PCL-diols calculated by ^{1}H-NMR (Eq. 1), which is given in Table 3, has been used in Eq. (7).

In this study, the hard segment content is fixed for all TPU samples, which leads to changes in the molar ratio

Table 3 Calculation of the number-average molecular weights of synthesized PCL-diols

Sample	A (δ_D)	A (δ_E)	X_{SS}	M_n calculated by ^{1}H-NMR
PCL 2000	1.00	8.98	17.96	2312
PCL 4000	1.00	18.58	37.16	4503
PCL 10000	1.00	46.23	92.46	10,815

and weight of the precursor. An increase in M_W for PCL-diol leads to an increase in the molar ratio of precursors. The increase in the number of moles of IPDI and BDO indicates the increase in the molecular weight of the resultant TPU polymer.

Gas permeability measurements

A gas permeation device measured the permeability of CO_2 and N_2 gas. Figure 3 is a schematic of this device. This device performs the permeability test at variable pressures at a constant volume. This measurement was performed at pressures of 3, 6, and 9 atm and ambient temperature. Each experiment was repeated at least three times.

One method for evaluating the membrane performance is to measure pure gas permeates and calculate selectivity. Thus, a circular membrane with a diameter of 2.5 cm is placed in the membrane modulus; pure gas is passed under a certain pressure. A graduated bubble cylinder calculates the volumetric gas flow through the membrane. To achieve a steady-state flow and compute the permeability (Eq. 8), the membranes are exposed to the gas flow for around 0.5–4 h. The samples are exposed to the gas flow for around 0.5–4 h. Giving more time and different filters in the gas path led to a stable state [18–21].

$$P = \frac{vl}{A \times (P_{feed} - P_{permeate})} \tag{8}$$

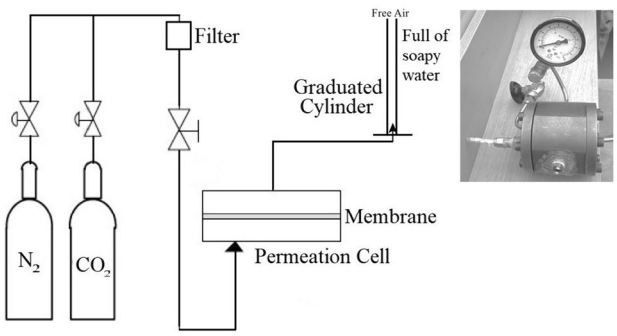

Fig. 3 Schematic view of gas permeation device

Here, P according to Barrer (1×10^{-10} cm^3 (STP)·cm/cm^2·s·cmHg) indicates the permeability of gas through the membrane, P_{feed} (cmHg) is the relative feed pressure, $P_{permeate}$ (cmHg) is the relative flow pressure, ν (cm^3/s) is the volumetric flow rate, A (cm^2) is the effective membrane surface area, and l (cm) is the thickness of the membrane.

Furthermore, the selectivity (α) of CO_2 relative to N_2 is defined as the ratio between the permeability of the two gases (Eq. 9) [22–25].

$$\alpha = \frac{P_{CO2}}{P_{N2}} \tag{9}$$

Results and discussion

^{1}H-NMR analysis of synthesized PCL-diols and TPUs

^{1}H-NMR analysis confirms the chemical structure of synthesized PCL-diols and TPUs. The chemical structures associated with the different protons are demonstrated in Figs. 4 and 5. Intensifications in PCL-diol at $\delta_A = 1.38$–1.42 ppm (–CH_2–CH_2–CH_2–), $\delta_B = 1.59$–1.69 ppm (–CH_2–CH_2–O), $\delta_C = 2.29$–2.32 ppm (–CH_2COO), $\delta_E = 4.04$–4.10 ppm (CH_2OCO) appear in repeating groups. The terminal group of PCL-diols is identified in $\delta_D = 3.62$–3.66 ppm (CH_2OH). The results of the ^{1}H-NMR spectra showed that PCL-diol was successfully synthesized and followed the proposed structure of Fig. 4 for PCL-diol. The results for PCL-diols are given in Table 3. The peaks appeared in $\delta = 7$–7.3 ppm for $CDCL_3$ as a solvent and in $\delta = 0.04$–0.09 ppm for the TMS marker [29, 33–35].

For TPUs, the methyl (CH_3) and methylene (CH_2) groups of IPDI and PCL-diol are found in $\delta = 0.88$–1.85 ppm. The methylene and methine groups attached to the nitrogen atom are found in $\delta = 2.13$–3.01 ppm. Methine and methylene groups attached to the urethane oxygen atom were identified at about $\delta = 4.2$–4.6 ppm, respectively [8]. Successful synthesizing of the TPUs was evaluated by the ^{1}H-NMR spectrum (Fig. 5).

FTIR analysis of synthesized PCL-diols and TPUs

FTIR spectra were used to study the chemical structure of PCL diols and TPUs. As discussed, the PCL-diol structure (Fig. 6) has three important functional groups. The peak (broad absorption) at the wave number range (3300–3600 cm^{-1}) corresponds to O–H stretching, and the peaks in the range (2800–3200 cm^{-1}) are related to C–H stretching. A sharp peak (strong absorption) in the range (1680–1750 cm^{-1}) is attributed to the carbonyl group (–C = O). Two peaks, one stronger than the other in the wave

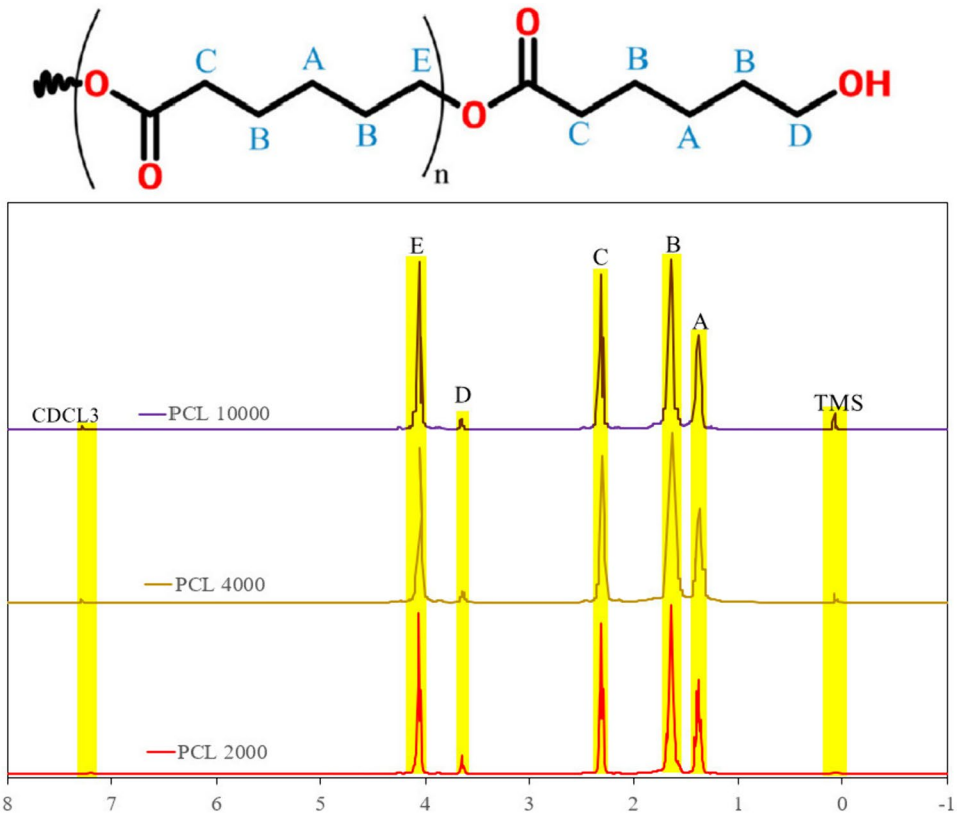

Fig. 4 ^{1}H-NMR spectra of synthesized PCL-diols with various molecular weights

number range (1100–1300 cm^{-1}), are related to C–O groups. The peaks at the wave number range (600–800 cm^{-1}) are related to the long chain band. Peaks in the wave number range (1368–1370 cm^{-1}) are related to $–CH_3$ bending. Peaks in the wave number range (1470–1472 cm^{-1}) with medium intensity are related to CH_2 bending [29, 33–35].

TPU structure was confirmed by the three main regions in FTIR spectroscopy (Fig. 7). Peaks in the wave numbers (3200–3400 cm^{-1}) belong to the –NH stretching containing hydrogen bonding and non-bonding. Wave numbers (2800–2950 cm^{-1}) belong to the –C–H (sp^3 hybridization) symmetric (2900 cm^{-1}) and asymmetric (2950 cm^{-1}). Two

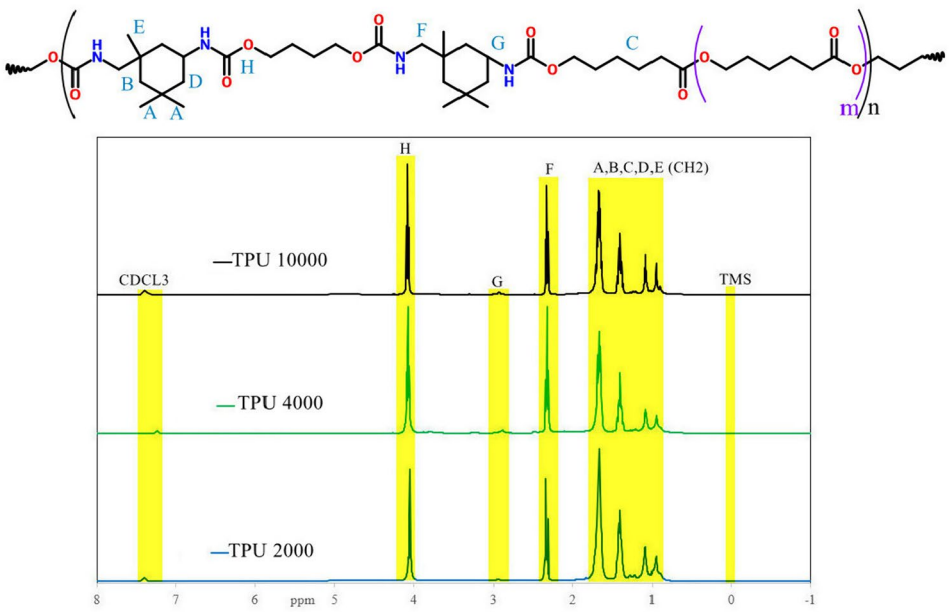

Fig. 5 ^{1}H-NMR spectra of synthesized TPUs

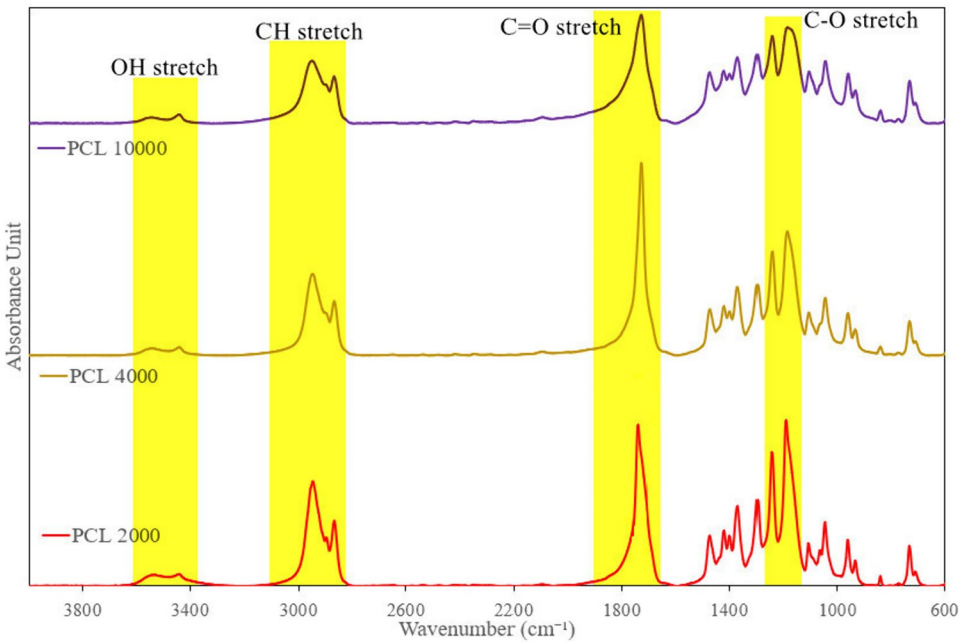

Fig. 6 FTIR spectra of synthesized PCL-diols

sharp peaks in wave numbers (1680–1730 cm^{-1}) are attributed to the free carbonyl groups (C = O) and hydrogen-bonded carbonyl groups. The peak corresponds to the free carbonyl group observed at 1720–1725 cm^{-1}, and the peak related to the hydrogen-bonded carbonyl group is observed at 1680–1690 cm^{-1}. The area below the free carbonyl and the hydrogen bond carbonyl peaks were deconvoluted using peak fit software. The values of HBI were investigated as an indicator of the amount of C = O with hydrogen bonds [29, 33–36].

Table 4 summarizes the HBI for various TPUs. The rest of the peaks that can be seen in Fig. 7. The peaks in the wave number range (1160–1165 cm^{-1}) are related to C–N bending. The peaks in the wavenumber range (1360–1365 cm^{-1}) are related to $–CH_3$ bending. The peaks in the range of wavenumber (1463–1466 cm^{-1}) are related to $–CH_2$ bending.

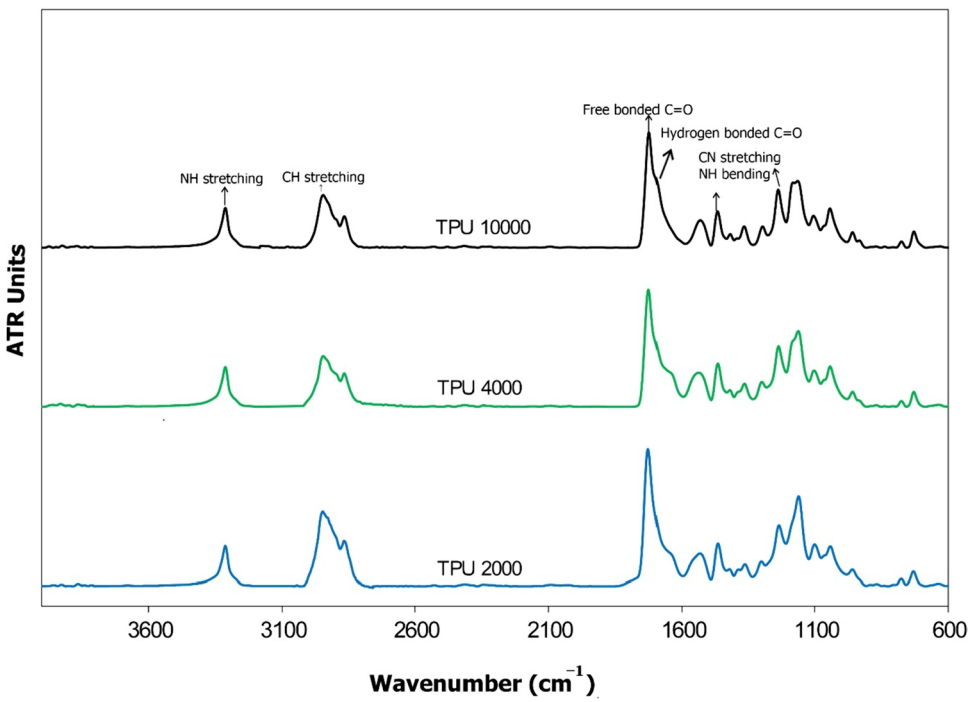

Fig. 7 FTIR spectra of synthesized TPUs

Table 4 HBI, degree of crystallinity, and crystal size for crystal plates of (110) and (200) in different PCL-diol and TPU samples were calculated by FTIR and XRD experiments

Sample	$A_{c=o\ bonded}$	$A_{c=o\ free}$	HBI (%)	L_{110} (nm)	L_{200} (nm)	Degree of crystallinity (%)
PCL 2000	N.O.[a]	N.O.[a]	N.O.[a]	27.38 ± 1.78	22.91 ± 1.21	51.85 ± 1.39
PCL 4000	N.O.[a]	N.O.[a]	N.O.[a]	31.50 ± 1.43	24.99 ± 1.01	49.19 ± 1.24
PCL 10000	N.O.[a]	N.O.[a]	N.O.[a]	39.12 ± 1.83	32.91 ± 0.87	42.74 ± 1.17
TPU 2000	5.12 ± 0.46	8.63 ± 0.49	17.55 ± 0.04	N.O.[b]	N.O.[b]	N.O.[b]
TPU 4000	6.32 ± 0.51	8.75 ± 0.45	37.24 ± 0.4	19.55 ± 0.88	17.18 ± 0.56	10.82 ± 1.44
TPU 10000	7.35 ± 0.53	8.83 ± 0.47	45.43 ± 0.05	16.83 ± 1.01	16.25 ± 0.55	20.16 ± 1.66

N.O.[a]: all of them are free carbonyl

N.O.[b]: due to the low crystallinity, no pattern was observed

The peaks in the wavenumber range (1530–1533 cm^{-1}) are related to C–N stretching and –NH bending vibrations. The peaks in the wavenumbers range (1100–1104 cm^{-1}) are related to C–O stretching. The peaks in wavenumbers (1234–1300 cm^{-1}) are related to O = C–O stretching vibrations of the ester group [29, 33–36].

As mentioned, TPUs comprise soft and hard segments and two types of hydrogen bonds between these segments. The hydrogen bonds are conducted between the hard segments (NH and CO of urethane) and between the hard and soft segments (NH and CO of ester). The first hydrogen bonding creates phase separation between hard and soft domains, and the second leads to phase mixing. Hydrogen bonds exist because of the structure of TPUs. The urethane carbonyl groups (in the hard segment) and the PCL-diol carbonyl groups (in the soft segment) act as proton acceptor groups and have hydrogen bonded with the NH groups in the hard segment, which act as proton donors [29, 33–36].

The increase in the molecular weight of PCL-diol leads to an increase in HBI. The hydrogen bonding of urethane–urethane is increased, which causes less phase mixing between hard and soft phases [29, 33–35].

XRD analysis of samples

X-Ray diffraction (XRD) analysis was used to examine the crystalline structure of the samples. For PCL-diols, three index peaks are observed in 2θ: (21, 22, 24)°, which corresponds to the crystal plates 110, 111, and 200, respectively (Figs. 8 and 9). The findings align with previous research

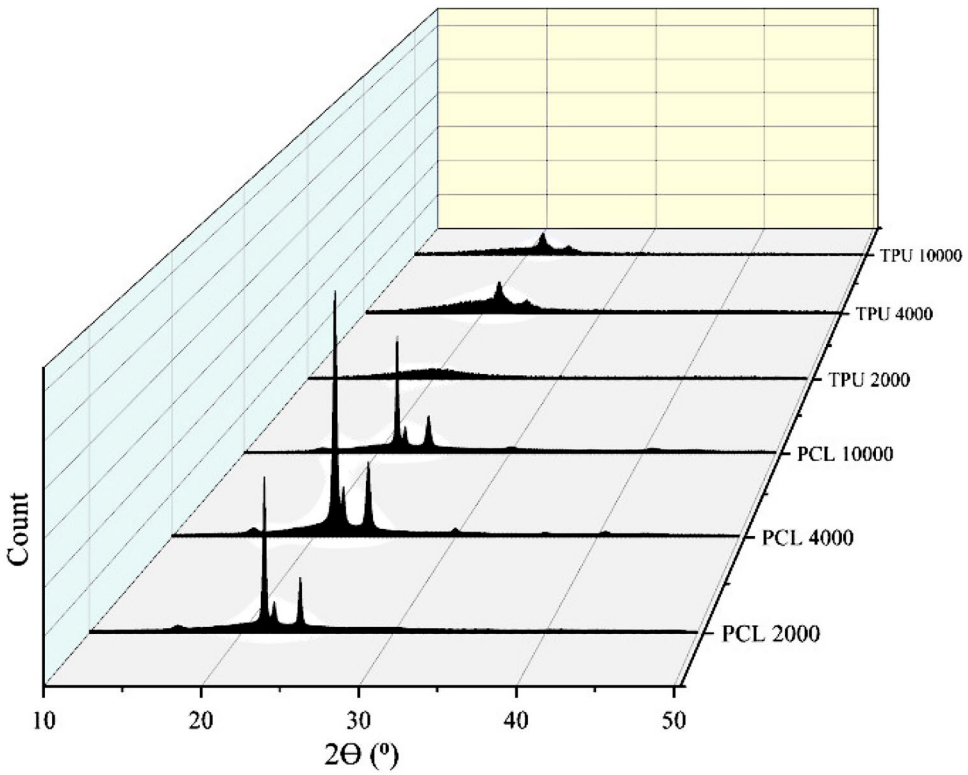

Fig. 8 XRD patterns of synthesized PCL-diol and TPU samples

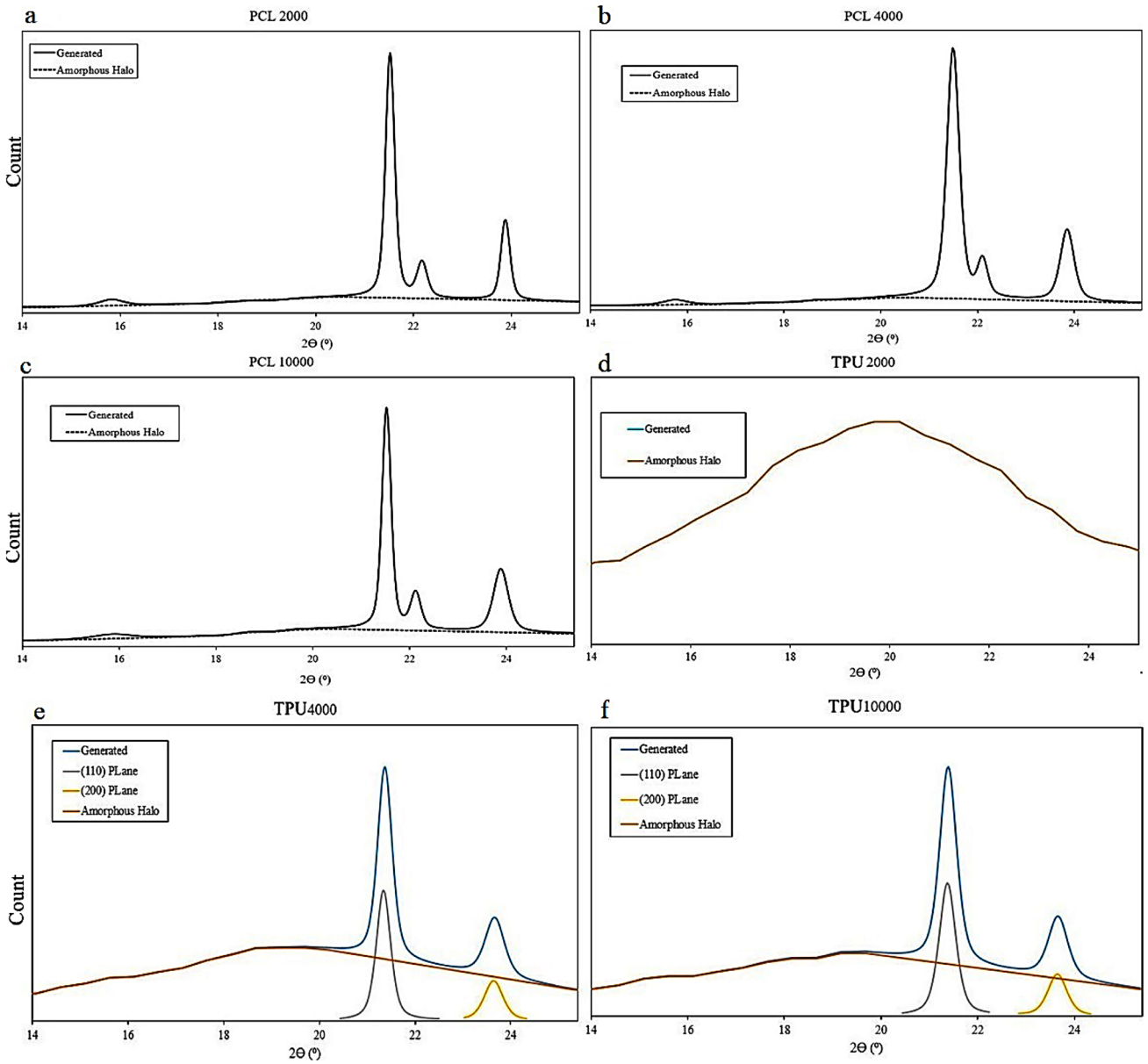

Fig. 9 XRD patterns of all samples, crystals with (110), (200) orientations, and amorphous halo of different samples

that verifies the crystalline nature of PCL-diol [29, 33–35]. Comparing the patterns of PCL-diol and TPU, some peaks have disappeared. The two significant peaks are observed as the two main reflections in TPUs (Figs. 8 and 9). To measure the impact of altering the molecular weight of PCL-diol on the crystalline structure of the samples, the degree of crystallinity and the size of the crystals in the soft part of TPUs were determined [33–35].

Figure 8 shows the XRD patterns of the samples. In the TPU2000 sample, no significant XRD pattern is observed due to this polymer sample's very low crystallinity (amorphous) [33–35].

Calculations were performed for all samples (Eqs. 5 and 6). Note that the degree of crystallinity calculated by this method is volumetric, and the results may be different from the DSC method calculations. The data is different, but the method is the same. According to the results in Table 4, with increasing molecular weight of PCL-diols, the degree of crystallinity decreases due to the inhibition of hard segments against crystallization of PCL-diol in TPU chains, especially using soft-to-hard hydrogen bonding [29, 33, 34]. However, in TPUs, the situation is quite the opposite, so as the polymer chain increases, crystallinity increases due to the increase in phase separation [29, 33, 34]. As previously

Table 5 Degree of crystallinity (X_S), melting point (T_m), glass transition temperature (T_g), and heat of fusion (ΔH_{SS}) of PCL-diols and TPUs determined by DSC

Sample		T_g (°C)	T_m (°C)	ΔH_{SS} (J/g)	X_c (%)
PCL diol	PCL 2000	− 58.63	50.56	82.01	60.30
	PCL 4000	− 57.12	55.35	79.13	58.18
	PCL 10000	− 56.47	57.98	78.57	57.77
TPU	TPU 2000	− 37.12	30.91	0.46	1.58
	TPU 4000	− 37.31	34.44	5.63	19.62
	TPU 10000	− 39.75	41.91	11.21	31.17

mentioned, from TPU2000 to TPU10000, the degree of phase separation is increased. The more phase separation, the less prevention imposed by hard segments on soft segments, resulting in a higher degree of crystallinity and increased crystal size.

DSC analysis

DSC analysis technique was used to investigate the thermophysical properties of the samples, and the results are given in Table 5 and Fig. 2. The DSC thermogram of PCL-diols has displayed two sharp peaks at temperature ranges of 48–57 °C and 19–28 °C, which can be assigned to the melting and crystallization of PCL-diol crystallites, respectively (Fig. 2a). For TPUs, it can be seen in the temperature range 30–41 °C corresponding to the melting point of polymer crystals. Also, the glass transition temperature (T_g) can be seen in the temperature range of − 37 to − 39 °C. For TPU in Fig. 2b, no transition has been seen for the hard phase at a temperature until 200 °C. It can be observed that the melting temperature is shifted to higher temperatures with increasing PCL-diol molecular weight [29, 33–35]. It can be observed that PCL-diol has higher T_m and % X_c. Constraints in the crystalline structure of the soft segments in the polymer chains have led to lower transition temperatures of TPU samples than PCL-diol. Hard domains in TPUs have prevented the crystallization of PCL-diols. Also, the interaction of hydrogen bonding between the carbonyl groups of PCL-diol from the soft part with the urethane groups (–NH) from the hard part has hindered the crystallization of PCL-diol in TPU. It can be assumed by comparing the relative crystallinity of the soft parts, a criterion for the microphase separation of TPUs. More microphase mixing between the hard and soft parts has imposed more restrictions on PCL-diol crystallization. Increasing the molecular weight of PCL-diol has led to less interphase mixing and more phase separation, resulting in increasing crystallinity in TPU [29, 33–35].

DSC analysis results confirm XRD calculations. DSC's calculated degree of crystallinity is the volumetric crystallinity, while XRD calculates mass crystallinity. The comparison results of Table 4 with Table 5 show that increasing and decreasing trends are the same. The heat of the fusion of soft parts was determined using the DSC test and Eq. (4) [29, 33–35].

According to the results of Table 6, the increase in the molecular weight of the soft segment (PCL-diol) leads to a decrease in the glass transition temperature (T_g) of TPUs. In the TPU structure, the PCL-diol chains are located between the hard segments, so their longer length leads to greater mobility. Therefore, the glass transition temperature for TPU shifts to higher temperatures as the molecular weight of PCL-diol increases [29, 33–35].

Mechanical properties

A tensile test was performed to evaluate the mechanical behavior of TPU membrane samples. As shown in Fig. 10 and Table 6, as the molecular weight of PCL-diol increases, the tensile strain decreases, and the tensile strength increases. It is observed that Young's modulus increases with the increasing molecular weight of PCL-diol (Table 6). As previously mentioned, increasing the molecular weight of PCL-diol increases HBI and the crystallinity of the soft segments. The most important factor in the mechanical properties of TPUs is HBI. Due to the increase in hydrogen bonding between the PU chains, an increase in tensile strength is observed. With increasing HBI, the phase separation between hard and soft segments is conducted, and the hydrogen bonds only occur between the hard domains, leading to an increment in Young's modulus. However, in this study, the HSC was kept constant by changing the molar ratio of precursors. It is found

Table 6 Young's modulus, elongation at the break, and yield stress of TPU membranes

Sample	Young's modulus (MPa)	Elongation at break (%)	Tensile strength (MPa)	Yield strain (%)	Yield stress (MPa)
TPU 2000	24.47	512.86	2.54	5.51	0.77
TPU 4000	496.68	449.65	15.49	3.26	6.82
TPU 10000	661.50	325.61	26.09	6.33	10.50

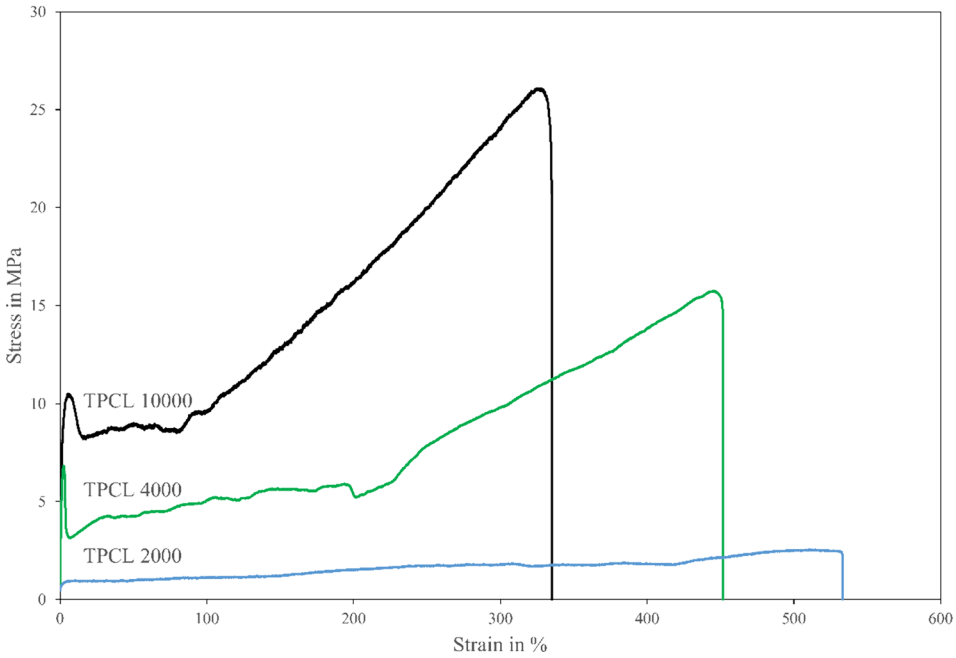

Fig. 10 Tensile stress–strain curves of prepared TPU membranes

that the mechanical properties of the TPU membrane are improved by increasing the molecular weight of PCL-diol [7, 17, 33, 34].

Gas permeation properties

The permeability of the membranes at a temperature of 25 °C and pressures of 3, 6, and 9 atm for CO_2 and N_2 gas were measured independently. In Fig. 11, the permeability of the gas through the membrane can be seen. It is observed that the permeation of CO_2 is higher than N_2 in all membranes. As mentioned in the "Introduction" section, the gas permeation mechanism occurs in three stages: the adsorption of gas molecules, the diffusion of gas molecules, and the desorption of gas molecules through the membrane's outer surface. The permeation content of gas

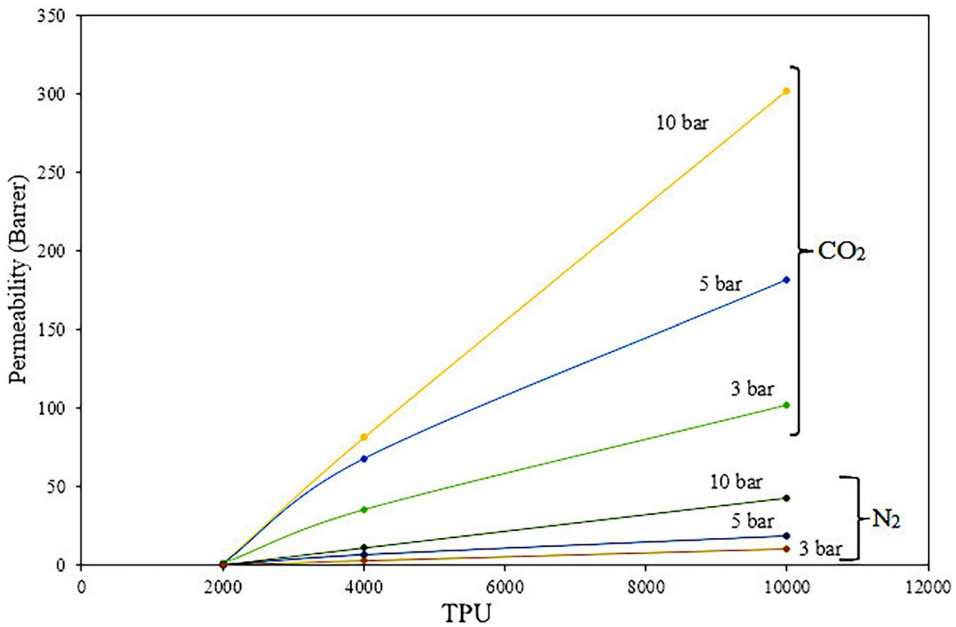

Fig. 11 Variation of permeability in TPU membranes with pressure for CO_2 and N_2 gases. The lines are used to guide the eyes

Table 7 Permeability of TPU samples

Permeability (Barrer)				
Gas	Sample	Pressure (atm)		
		3	6	9
CO_2	TPU 2000	7.33	8.12	9.54
	TPU 4000	34.97	67.64	81.28
	TPU 10000	101.50	181.26	302.48
N_2	TPU 2000	0.01	0.02	0.03
	TPU 4000	2.56	6.35	10.76
	TPU 10000	9.86	17.93	42.24

such as CO_2 through the polymeric membrane relates to its dissolution behavior in polymers. In the polymer structure, the presence of carbonyl groups causes further dissolution of CO_2 gas in the TPU membrane. It is observed that with increasing PCL-diol molecular weight, this dissolution and, consequently, permeability is increased. CO_2 is a weak electrophile that tends to receive electrons. Increased molecular weight and, consequently, hydrogen bonding in TPUs can be determining factors in increasing CO_2 dissolution in TPU membranes [7, 10, 13].

The permeability and selectivity of gas are given in Table 7 and 8. For TPU2000, it is observed that it has less permeability for both gases. Less phase separation, low polymer chain mobility, and low HBI have resulted in less gas permeability. However, the selectivity of CO_2 gas is higher than N_2. At a certain pressure, increasing the polymer chain lengths (due to the increase in the molecular weight of PCL-diols) has improved the gas permeability but reduced the selectivity [4, 16, 24–26].

In addition, increasing the gas pressure caused enhancement of the permeability and decline of the selectivity due to the improvement of the solubility of N_2 and CO_2 gas in TPU membranes. However, the change in the rate of dissolution of CO_2 in TPU with pressure variations is higher than N_2 due to the higher affinity of CO_2 to urethane and carbonyl groups of TPU compared to N_2 gas [4, 14, 16, 17, 24–26].

Table 8 Selectivity of TPU samples

Selectivity ($\alpha_{CO2/N2}$)			
Sample	Pressure (atm)		
	3	6	9
TPU 2000	45.33	36.36	27.14
TPU 4000	13.65	10.65	7.55
TPU 10000	10.29	10.11	7.16

Conclusions

Thermoplastic polyurethanes containing 30 wt.% HSCs were synthesized using IPDI as diisocyanate, BDO as the chain extender, and PCL-diol with different molecular weights as a polyol. PCL-diols by different M_W (2000, 4000, and 10,000 g/mol) were adjusted and used in TPU synthesis. The ^{1}H-NMR and FTIR spectra showed that PCL-diol and TPU were successfully synthesized. In addition, FTIR spectra manifested that the increasing molecular weight of PCL-diol caused an enhancement of the hydrogen bonding index (HBI) in TPU, which led to an increase in phase separation. XRD analysis showed a decrease in the crystallinity of the samples with PCL-diol molecular weight increment, confirmed by the DSC thermograms. The tensile tests revealed that the increase in the M_W of the PCL-diol soft segments and in the HBI of TPU led to an increment in tensile strength and Young's modulus of TPU samples. In the gas permeability test, it was noticed that, at all pressures, the increase in M_W of PCL-diol due to the enhanced polymer chain length in TPUs led to the enhancement in permeability of CO_2 and N_2 gas. However, due to the saturation of CO_2 in the TPU membrane, the increase in molecular weight caused the selectivity to be decreased.

Author contribution All authors contributed to the research's design and implementation, the results analysis, and the manuscript's writing.

Funding The authors declare that no funds, grants, or other support were received during the preparation of this manuscript.

Availability of data and materials The data created, procured, or used for this research project can be accessed in this manuscript.

Declarations

Consent to participate All authors have participated in the conception, design, analysis, and interpretation of the data, drafting the article, or revising it critically for important intellectual content, and approving the final version.

Consent for publication All authors confirm that this manuscript has not been published elsewhere and is not under consideration by another journal.

Competing interests The authors declare no competing interests.

Disclosure This manuscript has not been submitted to, nor is it under review at, another journal or other publishing venue. The authors have no affiliation with any organization with a direct or indirect financial interest in the subject matter discussed in the manuscript. The authors have no relevant financial or non-financial interests to disclose.

.

References

1. Das C, Gebru KA (2018) Polymeric membrane synthesis, modification, and applications: electro-spun and phase inverted membranes. Taylor & Francis Group CRC Press, New York, pp 5–11, pp 21–23
2. Khulbe KC (2021) Nanotechnology in membrane processes. Springer Nature, Switzerland, pp 23–36
3. Karimi MB, Khanbabaei G, Sadeghi MM (2017) Vegetable oil-based polyurethane membrane for gas separation. J Mem Sci 527:198–206. https://doi.org/10.1016/j.memsci.2016.12.008
4. Joshi M, Adak B, Butola BS (2018) Polyurethane nanocomposite-based gas barrier films, membranes, and coatings: a review on synthesis, characterization, and potential applications. Prog Mater Sci 97:230–282. https://doi.org/10.1016/j.pmatsci.2018.05.001
5. Dolmaire N, Méchin F, Espuche É (2006) Water transport in polyurethane/polydimethylsiloxane membranes: influence of the hydrophobic/hydrophilic balance and of the crosslink density. Desalination 199(1–3):118–120. https://doi.org/10.1016/j.desal.2006.03.154
6. Wypych G (2022) Handbook of polymers. Elsevier, Canada, pp 579–584, pp 665–668
7. Drobny JG (2014) Handbook of thermoplastic elastomers. Elsevier, New Jersey, pp 9–16, pp 215–221
8. Mansouri M, Ghadimi A, Gharibi R, Norouzbahari S (2021) Gas permeation properties of highly cross-linked castor oil-based polyurethane membranes synthesized through thiol-yne click polymerization. React Funct Polym 158:104799. https://doi.org/10.1016/j.reactfunctpolym.2020.104799
9. Maher BM, Rezaali J, Ghaleh H et al (2017) Evaluation of poly (2-hydroxyethyl methacrylate) and poly (methyl methacrylate)-grafted poly (vinylidene fluoride)-poly (dimethyl siloxane) bilayers for gas separation. Colloid Polym Sci 295(9):1595–1607. https://doi.org/10.1007/s00396-017-4124-7
10. Eusébio TM, Martins AR, Pon G et al (2020) Sorption/diffusion contributions to the gas permeation properties of bi-soft segment polyurethane/polycaprolactone membranes for membrane blood oxygenators. Membranes 10(1):8. https://doi.org/10.3390/membranes10010008
11. Low SC, Murugaiyan SV (2021) Thermoplastic polymers in membrane separation. https://doi.org/10.1016/B978-0-12-820352-1.00083-3
12. Melnig V, Apostu MO, Tura V, Ciobanu C (2005) Optimization of polyurethane membranes: morphology and structure studies. J Membr Sci 267(1–2):58–67. https://doi.org/10.1016/j.memsci.2005.04.054
13. Shahzamani M, Ebrahimi NG, Sadeghi M, Mostafavi F (2016) Relationship between the microstructure and gas transport properties of polyurethane/polycaprolactone blends. IJChE 13(3):78–88
14. Baker RW (2004) Membrane technology and applications. John Wiley & Sons, California, pp 9–16, pp 215–221
15. Wolińska-Grabczyk A (2006) Effect of the hard segment domains on the permeation and separation ability of the polyurethane-based membranes in benzene/cyclohexane separation by pervaporation. J Membr Sci 282(1–2):225–236. https://doi.org/10.1016/j.memsci.2006.05.026
16. Semsarzadeh MA, Sadeghi M, Barikani M (2007) The effect of hard segments on the gas separation properties of polyurethane membranes. Iran Polym J 16(12):819–827
17. Maghsoud Z, Pakbaz M, Famili MHN, Madaeni SS (2017) New polyvinyl chloride/thermoplastic polyurethane membranes with potential application in nanofiltration. J Membr Sci 541:271–280. https://doi.org/10.1016/j.memsci.2017.07.001
18. Szycher M (2013) Polyurethanes. Taylor & Francis Group CRC Press, New York, pp 1–6, pp 41–50
19. Fakhar A, Sadeghi M, Dinari M, Lammertink R (2019) Association of hard segments in gas separation through polyurethane membranes with aromatic bulky chain extenders. J Membr Sci 574:136–146. https://doi.org/10.1016/j.memsci.2018.12.062
20. Sadeghi M, Talakesh MM, Arabi Shamsabadi A, Soroush M (2018) Novel application of a polyurethane membrane for efficient separation of hydrogen sulfide from binary and ternary gas mixtures. ChemistrySelect 3(11):3302–3308. https://doi.org/10.1002/slct.201703170
21. Santos GH, Rodrigues MA, Ferraz HC, Moura LC, de Miranda JL (2019) A more sustainable polyurethane membrane for gas separation at room temperature and low pressure. In Materials Science Forum 965:125–132. https://doi.org/10.4028/www.scientific.net/MSF.965.125
22. Fakhar A, Sadeghi M, Dinari M et al (2020) Elucidating the effect of chain extenders substituted by aliphatic side chains on morphology and gas separation of polyurethanes. Eur Polym J 122:109346. https://doi.org/10.1016/j.eurpolymj.2019.109346
23. Norouzbahari S, Gharibi R (2020) An investigation on structural and gas transport properties of modified cross-linked PEG-PU membranes for CO_2 separation. React Funct Polym 151:104585. https://doi.org/10.1016/j.reactfunctpolym.2020.104585
24. Turan D, Sängerlaub S, Stramm C, Gunes G (2017) Gas permeabilities of polyurethane films for fresh produce packaging: response of O_2 permeability to temperature and relative humidity. Polym Test 59:237–244. https://doi.org/10.1016/j.polymertesting.2017.02.007
25. Isfahani AP, Sadeghi M, Wakimoto K et al (2017) Enhancement of CO_2 capture by polyethylene glycol-based polyurethane membranes. J Membr Sci 542:143–149. https://doi.org/10.1016/j.memsci.2017.08.006
26. Adam NI, Hanibah H, Subban RHY et al (2020) Palm-based cationic polyurethane membranes for solid polymer electrolytes application: a physico-chemical characteristics studies of chain-extended cationic polyurethane. Ind Crop Prod 155:112757. https://doi.org/10.1016/j.indcrop.2020.112757
27. Sadeghi M, Semsarzadeh MA, Barikani M, Ghalei B (2011) Study on the morphology and gas permeation property of polyurethane membranes. J Membr Sci 385:76–85. https://doi.org/10.1016/j.memsci.2011.09.024
28. Liu L, Huang ZM, He CL, Han XJ (2006) Mechanical performance of laminated composites incorporated with nanofibrous membranes. Mater Sci Eng 435:309–317. https://doi.org/10.1016/j.msea.2006.07.064
29. Eusébio TM, Faria M, Filipe EJ, de Pinho MN (2019) Polyurethane urea membranes for membrane blood oxygenators: synthesis and gas permeation properties. ENBENG 1–4 IEEE
30. Babaie A, Rezaei M, Sofla RLM (2019) Investigation of the effects of polycaprolactone molecular weight and graphene content on crystallinity, mechanical properties, and shape memory behavior of polyurethane/graphene nanocomposites. J mech behav of biomed 96:53–68. https://doi.org/10.1016/j.jmbbm.2019.04.034
31. Storey RF, Sherman JW (2002) Kinetics and mechanism of the stannous octoate-catalyzed bulk polymerization of ε-caprolactone. Macromolecules 35(5):1504–1512. https://doi.org/10.1021/ma010986c
32. Lipik VT, Abadie MJ (2010) Process optimization of poly (ε-caprolactone) synthesis by ring-opening polymerization. Iran Polym J 19(11):885–893
33. Crescenzi V, Manzini G, Calzolari G, Borri C (1972) Thermodynamics of fusion of poly-β-propiolactone and poly-ϵ-caprolactone. Comparative analysis of the melting of aliphatic polylactone and polyester chains. Eur Polym J 8(3):449–463. https://doi.org/10.1016/0014-3057(72)90109-7
34. Eyvazzadeh Kalajahi A, Rezaei M, Abbasi F (2016) Preparation, characterization, and thermomechanical properties of poly

(ε-caprolactone)-piperazine-based polyurethane-urea shape memory polymers. Mater Sci 51(9):4379–4389. https://doi.org/10.1007/s10853-016-9750-9

35. Eyvazzadeh Kalajahi A, Rezaei M, Abbasi F, Mir Mohamad Sadeghi G (2017) The effect of chain extender type on the physical, mechanical, and shape memory properties of poly (ε-caprolactone)-based polyurethane-ureas. Polym Plast Tech Eng 56(18):1977–1985. https://doi.org/10.1080/03602559.2017.1298797
36. Puszka A, Sikora JW, Nurzyńska A (2024) Influence of the type of soft segment on the selected properties of polyurethane materials for biomedical applications. Materials 17(4):840. https://doi.org/10.3390/ma17040840